Symbolic Quantum-Trajectory Method for Multichannel Dicke Superradiance

Raphael Holzinger,[1,2,*] Nico S. Bassler,[3] Julian Lyne,[4,5] Susanne F. Yelin,[2] and Claudiu Genes[3,4,†]
[1]Institute for Theoretical Physics, University of Innsbruck, Technikerstraße 21a, A-6020 Innsbruck, Austria
[2]Department of Physics, Harvard University, Cambridge, Massachusetts 02138, USA
[3]TU Darmstadt, Institute for Applied Physics, Hochschulstraße 4A, D-64289 Darmstadt, Germany
[4]Max Planck Institute for the Science of Light, Staudtstraße 2, D-91058 Erlangen, Germany
[5]Department of Physics, Friedrich-Alexander Universität Erlangen-Nürnberg (FAU), Staudtstraße 7, D-91058 Erlangen, Germany

(Received 28 November 2025; accepted 21 October 2026; published 6 November 2026)

We solve Dicke superradiance with two or more competing collective decay channels of tunable rates using a symbolic quantum-trajectory construction. The method yields closed time-domain populations and observables as finite combinations of exponential terms for arbitrary numbers of emitters and arbitrary decay rates. For two channels, the behavior of the stationary ground-state distribution resembles a first-order phase transition at the point where the channel-rate ratio is equal to unity. For balanced d-channel decay, we obtain scaling laws for the superradiant peak time and intensity. These results unify and extend single-channel Dicke dynamics to multilevel emitters and provide a compact tool for cavity and waveguide experiments, where permutation-symmetric reservoirs engineer multiple collective decay paths.

DOI: 10.1103/5qcc-wfv6

Collective light-matter coupling is a cornerstone of quantum optics, with Dicke's seminal prediction of superradiance standing as its most striking manifestation [1]. When an ensemble of N identical two-level emitters is fully inverted, the sample releases a superradiant burst whose peak intensity scales quadratically, $I_{\max} \propto N^2$, and occurs at $t_{\text{peak}} \simeq \ln N/(\gamma N)$, where γ is the single-atom decay rate [2,3]. Closed, time-domain solutions of this single-channel problem were obtained in the 1970s [4,5] and by different methods, more recently [6,7].

Real emitters, however, are rarely ideal two-level systems. Many atomic, molecular, and solid-state emitters possess multiple stable ground sublevels. Collective decay of the different optical branches is most faithfully described by Eq. (1) when the emitters couple to a common engineered reservoir, such as a lossy cavity mode or a guided mode of a waveguide. Subwavelength free-space ensembles can also exhibit collective emission, but generally feature additional dipole-dipole interactions and short-range coherent photon exchange that are not included in the permutation-symmetric dissipative model considered here. In the collective-reservoir setting, every branch $|e\rangle \to |g_\alpha\rangle$ can radiate collectively, yielding a multinomial web of decay paths. Analytical results for such *multichannel* superradiance exist only in narrow limits—one dominant channel, in the limit of large N, or full numerical diagonalization of the Liouvillian superoperator for a few emitters [8–12]. A general closed-form solution has been missing.

We provide such a solution for N identical, initially fully excited emitters with one excited state $|e\rangle$ and a d-fold ground manifold $\{|g_1\rangle, \ldots, |g_d\rangle\}$. In the absence of driving, the density matrix obeys the permutation-symmetric Lindblad equation,

$$\dot{\hat{\rho}} = \sum_{\alpha=1}^{d} \Gamma_\alpha \mathcal{D}[\hat{S}_\alpha]\hat{\rho}, \qquad \hat{S}_\alpha = \sum_{j=1}^{N} |g_\alpha^{(j)}\rangle\langle e^{(j)}|, \tag{1}$$

where $\mathcal{D}[\hat{C}]\hat{\rho} = \hat{C}\hat{\rho}\hat{C}^\dagger - \frac{1}{2}\{\hat{C}^\dagger\hat{C}, \hat{\rho}\}$. Because the collective jump operators $\hat{S}_\alpha$ commute with particle permutations and we start in the fully symmetric state $|e\rangle^{\otimes N}$, the dynamics remain in the symmetric subspace where $\hat{S}_\alpha$ are the lowering operators for $\mathrm{SU}(d+1)$ with known matrix elements. The Hilbert-space dimension grows only polynomially with N, as $\binom{N+d}{d}$.

Permutation symmetry has been exploited more generally to reduce the numerical complexity of open many-body dynamics, including permutation-invariant master-equation approaches [13–15] and quantum-trajectory formulations in symmetry-reduced Dicke spaces [16,17]. The additional simplification exploited here is that the present undriven collective-decay dynamics form a directed, acyclic cascade in excitation number, while the no-jump evolution is diagonal in the symmetric Dicke basis. The ordered

*Contact author: raphael.holzinger@uibk.ac.at
†Contact author: claudiu.genes@physik.tu-darmstadt.de

Published by the American Physical Society under the terms of the Creative Commons Attribution 4.0 International license. Further distribution of this work must maintain attribution to the author(s) and the published article's title, journal citation, and DOI.

jump-time integrals can therefore be evaluated analytically as finite convolutions, or equivalently as rational functions in Laplace space. Thus, permutation symmetry provides the reduced state space, whereas the acyclic trajectory structure enables the closed analytical solution.

We derive a closed time-domain expression for $\hat{\rho}(t)$ valid for arbitrary N and arbitrary decay rates $\{\Gamma_\alpha\}$. Our approach is built on a symbolic quantum-trajectory (quantum-jump) construction [18–20], adapted to the multichannel case. All observables, populations, intensities, and higher-order correlations can then be obtained analytically from the resulting finite trajectory expressions.

Previous work on multilevel superradiant dynamics has shown, for example, cavity-mediated decay of multilevel atoms into permutation-symmetric entangled dark states [9]. Mok *et al.* analyzed many-body decay with competing branches and proved a "winner-takes-all" ground-state selection from a hydrodynamic continuum description [11]. In contrast, we obtain exact closed solutions of the d-channel Dicke master equation via a symbolic trajectory construction, giving full transient dynamics and exact stationary state distributions for any N, which are not available in Refs. [9,11]. Note that the stationary state here refers to the $t \to \infty$ limit of the undriven Lindblad dynamics, which depends on the initial state.

Figure 1(a) illustrates a possible implementation of multichannel Dicke superradiance via lossy cavity modes resonant with the emitters' decay branches. These modes act as permutation-symmetric reservoirs that funnel all radiation into collective channels [21]. For resonant cavity modes with decay rates κ_α coupled with strengths $\tilde{g}_\alpha$ to transitions $|e\rangle \to |g_\alpha\rangle$, adiabatic elimination in the bad-cavity regime $\kappa_\alpha \gg \tilde{g}_\alpha$ yields a purely dissipative Dicke master equation with collective jump operators $\hat{S}_\alpha$ and cavity-tuned rates $\Gamma_\alpha = 4\tilde{g}_\alpha^2/\kappa_\alpha$, without collective Lamb shift (it vanishes at resonance; see Supplemental Material [22]). Two orthogonal polarizations of a single cavity, or two crossed cavities, generate a two-channel scenario with independently tunable rates $\Gamma_{1,2}$ and adjusting $\tilde{g}_\alpha$ (or κ_α) sets the ratio $r = \Gamma_2/\Gamma_1$ that controls the stationary state ground-state distribution in Figs. 1(b) and 1(c). For large N this leads to a sharp transition around the balanced decay point $r = 1$, where the ground-state distribution is flat, in contrast to the binomial distribution for independent decay. The cavity setup is a far more faithful implementation of the model Eq. (1) than emitters in a small volume, where the vectorial character of the dipolar interactions and the diverging short-range unitary photon exchange complicate the dynamics.

Dicke superradiance in the bad-cavity regime has been realized with cold atoms (steady-state Raman superradiant lasers and ultranarrow Sr transitions) and in circuit QED with artificial atoms in fast-decaying cavities [23–27]. Multichannel Dicke superradiance can also be realized in one-dimensional nanophotonic waveguide QED

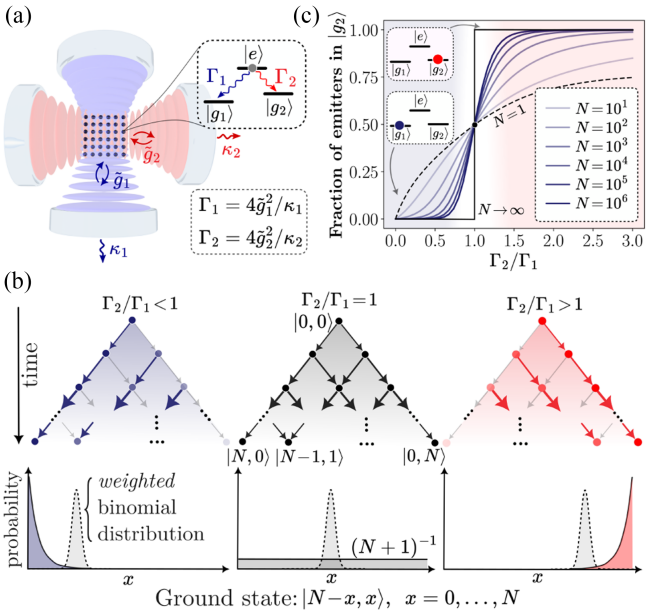


FIG. 1. (a) Two-channel Dicke superradiance engineered by two lossy cavity modes acting as permutation-symmetric reservoirs. Each mode couples resonantly to a transition of N Λ-type emitters with strengths $\tilde{g}_\alpha$ and cavity decays κ_α, giving collective decay rates $\Gamma_\alpha = 4\tilde{g}_\alpha^2/\kappa_\alpha$ in the bad-cavity limit $\kappa_\alpha \gg \tilde{g}_\alpha$. (b) Competition within the ground-state manifold spanned by $\{|g_1\rangle, |g_2\rangle\}$, increasingly sensitive to the decay-rate ratio $r = \Gamma_2/\Gamma_1$ with growing N. Our symbolic trajectory method yields the full time evolution from the inverted state, through the burst, to the stationary state distribution of Eq. (9), in contrast to the weighted binomial distribution for independently decaying emitters. For independent decay $|N-x,x\rangle$ denotes product states $|g_1\rangle^{\otimes(N-x)} \otimes |g_2\rangle^{\otimes x}$. (c) In the limit $N \to \infty$ the fraction of emitters in $|g_2\rangle$ exhibits a sharp change around $r = 1$.

platforms [28–33], where guided modes provide permutation-symmetric reservoirs. In Supplemental Material [22] we show the adiabatic elimination of multiple cavity modes and its validity in the bad-cavity limit.

Introducing the symbolic quantum-trajectory method—We first introduce the symbolic quantum-trajectory method for a single jump operator with rate Γ, corresponding to single-channel Dicke superradiance, for which analytical solutions are known [6,7]. The method yields an exact time-domain form of $\hat{\rho}(t)$ obtained from quantum trajectories. The stochastic unraveling converts the Lindblad equation into an ensemble of pure-state trajectories [18,34,35]; here we summarize the elements needed.

In the quantum-jump picture, a trajectory is a sequence of nonunitary evolutions interrupted by instantaneous jumps. Let $\hat{S}$ be the collective collapse operator with rate Γ [Eq. (1) and Fig. 2(a)]. Between jumps the system evolves under $\hat{U}_{t,t'} = \exp[-i\hat{H}_{\text{eff}}(t-t')]$ with effective non-Hermitian Hamiltonian $\hat{H}_{\text{eff}} = -i(\Gamma/2)\hat{S}^\dagger\hat{S}$. Any additional diagonal term $\hat{H}_0$ (containing the level energies) commuting with $\hat{S}^\dagger\hat{S}$ would not affect the population

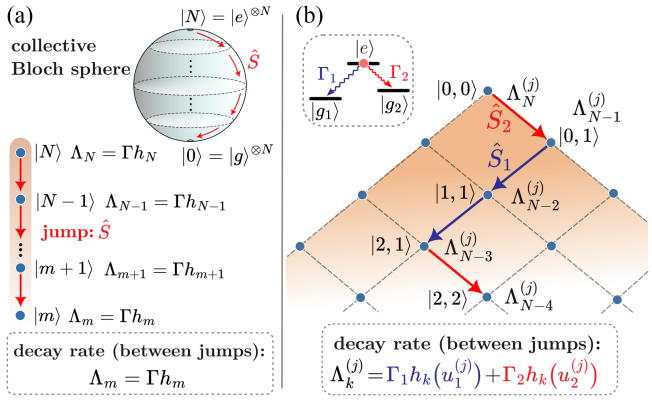


FIG. 2. (a) Single-channel Dicke superradiance. Decay cascade from the fully inverted state: non-Hermitian time evolution with rates Λ_m and successive jumps ($\hat{S}$) generate states $|m\rangle$ [Eq. (2)]. The dynamics reside on the surface of the collective Bloch sphere. (b) Two-channel Dicke superradiance. An inverted ensemble of N three-level systems with a twofold ground manifold decays through two collective channels at rates Γ_1, Γ_2. Starting from $|0,0\rangle$, a trajectory (j) with non-Hermitian evolution (rate $\Lambda_k^{(j)}$) and jumps ($\hat{S}_1$, $\hat{S}_2$) through states $|u_1^{(j)}, u_2^{(j)}\rangle$ ends in $|n_1, n_2\rangle$ [Eq. (12)]. The ground state is a distribution over $n_1 + n_2 = N$.

dynamics considered here. Let $\hat{S}$ act on Dicke states as $\hat{S}|m\rangle = \sqrt{h_m}|m-1\rangle$ with $h_m = m(N+1-m)$, where $|m\rangle$ denotes the symmetric Dicke state with m excitations. The density operator is diagonal in this basis, $\hat{\rho}(t) = \sum_{m=0}^{N} p_m(t)|m\rangle\langle m|$.

Consider a trajectory at time t starting from $|N\rangle$ at $t_0 = 0$ with exactly q jumps at times $t_0 < t_1 < \ldots < t_q < t$. After q jumps the state is $|m\rangle$ with $m = N - q$ excitations,

$$|\psi_q(t;\boldsymbol{t}_q)\rangle = \hat{U}_{t,t_q}\hat{S}\cdots\hat{S}\hat{U}_{t_2,t_1}\hat{S}\hat{U}_{t_1,t_0}|N\rangle, \tag{2}$$

where $\boldsymbol{t}_q = \{t_1, \ldots, t_q\}$ is the set of jump times. The q actions of $\hat{S}$ give the prefactor

$$\sqrt{\Gamma^{N-m}h_N\cdots h_{m+1}} = \sqrt{\frac{\Gamma^{N-m}N!(N-m)!}{m!}} = \sqrt{\mathcal{C}_m}, \tag{3}$$

where each collapse operator includes a factor $\sqrt{\Gamma}$ [18]. The $q+1$ non-Hermitian evolution operators yield a product of exponentials with decay rates of the visited states: $e^{-(\Gamma/2)h_{N-q}(t-t_q)}\cdots e^{-(\Gamma/2)h_N t_1}$.

The density operator is obtained by summing *all* trajectories and integrating over ordered jump times,

$$\hat{\rho}(t) = \sum_{q=0}^{N}\int_{0<t_1<\ldots<t_q<t} dt_1\ldots dt_q|\psi_q(t;\boldsymbol{t}_q)\rangle\langle\psi_q(t;\boldsymbol{t}_q)|. \tag{4}$$

The population $p_m(t)$ is therefore

$$p_m(t) = \mathcal{C}_m\int_{0<t_1<\ldots<t_q<t} e^{-\Lambda_m(t-t_q)}\cdots e^{-\Lambda_N t_1}dt_1\cdots dt_q, \tag{5}$$

where $q = N - m$ and with rates $\Lambda_m = \Gamma h_m$. More formally and compactly, we can rewrite the solution as a sequence of nested convolutions [using $(f*g)(t) = \int_0^t f(t-\tau)g(\tau)d\tau$ as the definition for convolutions],

$$p_m(t) = \mathcal{C}_m(e^{-\Lambda_N t} * \cdots * e^{-\Lambda_m t}). \tag{6}$$

Each convolution adds an exponential with the decay rate of the respective state. For a target state m the sequence contains $N - m + 1$ terms [Fig. 2(a)]. For states below half inversion, degeneracy $\Lambda_m = \Lambda_{N+1-m}$ leads to repeated terms, and by commutativity, one finds $e^{-\Lambda_m t} * e^{-\Lambda_{N+1-m}t} = te^{-\Lambda_m t}$. Alternatively, one may work in Laplace space,

$$\tilde{p}_m(s) = \mathcal{C}_m\prod_{k=m}^{N}\frac{1}{(s+\Lambda_k)}, \qquad p_m(t) = \frac{1}{2\pi i}\oint_{\mathcal{C}}\tilde{p}_m(s)e^{st}ds, \tag{7}$$

where $\mathcal{C}$ encircles all poles $s = -\Lambda_k$ counterclockwise. For m below the equator, $\Lambda_m = \Lambda_{N+1-m}$ yields double poles [6]. If $\{\Lambda_\alpha\} = \{\Lambda_k\colon k = m, \ldots, N\}$ is the set of distinct rates with multiplicities $\nu_\alpha \in \{1, 2\}$, one can equivalently replace $\tilde{p}_m(s)$ by $\mathcal{Q}_m(s) = \mathcal{C}_m\prod_\alpha(s+\Lambda_\alpha)^{-\nu_\alpha}$ [6,7].

For instance, the standard signature of superradiance, namely the emitted power, $\mathcal{I}(t) = \mathrm{Tr}\left[\Gamma\hat{S}^\dagger\hat{S}\hat{\rho}(t)\right]$ (in units of $\hbar\omega$), becomes

$$\mathcal{I}(t) = \sum_{m=0}^{N}\Lambda_m p_m(t) = \Gamma\sum_{m=0}^{N}m(N+1-m)p_m(t). \tag{8}$$

We illustrate the standard peak of superradiance ($d = 1$) and its extension to multiple decay channels in Fig. 3.

Two-channel Dicke superradiance—We now generalize to Dicke superradiance with two competing channels $|e\rangle \to |g_1\rangle$ and $|e\rangle \to |g_2\rangle$ with decay rates Γ_1 and Γ_2 and jump operators $\hat{S}_1$ and $\hat{S}_2$ defined in Eq. (1).

Since $\hat{S}_{1,2}$ commute with all particle permutations and the initial state $|e\rangle^{\otimes N}$ is symmetric, the dynamics reside in the symmetric subspace of $(\mathbb{C}^3)^{\otimes N}$. As in the single-channel case we track states with m excitations, starting from $m = N$. We label each symmetric Dicke state by the occupation numbers (n_1, n_2) of ground sublevels $|g_1\rangle, |g_2\rangle$, so that after q jumps we have $m = N - n_1 - n_2 = N - q$ excited emitters [Fig. 2(b)]. We define

$$|n_1, n_2\rangle = \mathcal{N}\sum_{\pi\in S_N}P_\pi(|e\rangle^{\otimes m}\otimes|g_1\rangle^{\otimes n_1}\otimes|g_2\rangle^{\otimes n_2}), \tag{9}$$

where P_π permutes emitters and S_N is the symmetric group.

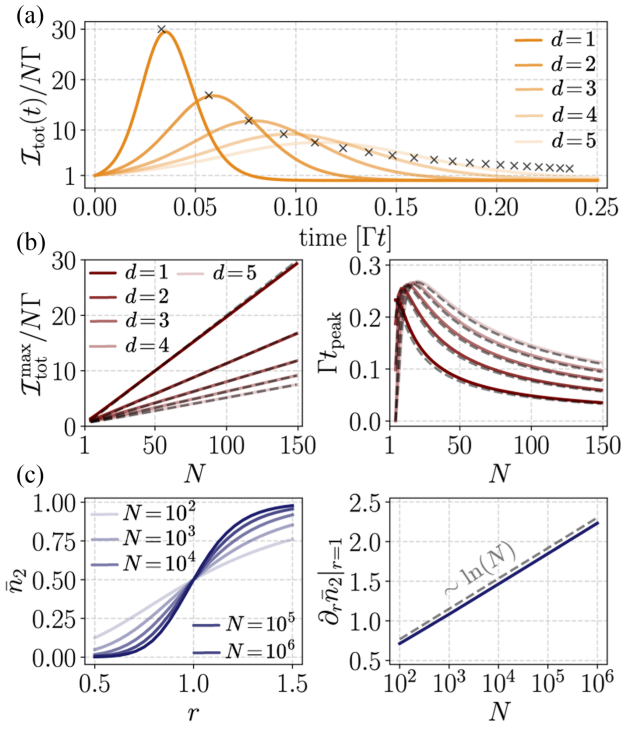


FIG. 3. (a) Emitted intensity versus time for increasing numbers of collective decay channels d with balanced rates $\Gamma_1 = \cdots = \Gamma_d = \Gamma/d$ for $N = 150$. As d grows, the burst weakens and is delayed. Crosses indicate analytic predictions for $(t_{\rm peak}, \mathcal{I}^{\rm max}_{\rm tot})$ from Eq. (16). (b) Total emitted peak intensity and peak time versus d from the analytic trajectory solution (Supplemental Material [22]). Dashed lines show the analytic scalings in Eq. (16). (c) Final population fraction $\bar{n}_2$ in $|g_2\rangle$ versus decay-rate ratio r. The order parameter changes sharply near $r = 1$, with analytic slope $\partial_r \bar{n}_2|_{r=1} \approx \ln(N)/6$ in Eq. (17).

The normalization $\mathcal{N} = \sqrt{m! n_1! n_2!/N!}$ ensures $\langle n_1', n_2' | n_1, n_2 \rangle = \delta_{n_1 n_1'} \delta_{n_2 n_2'}$.

We let the excitation number m run from N down to 0 and introduce counters $u_1 \in [0, n_1]$ and $u_2 \in [0, n_2]$. At each level m they obey $u_1 + u_2 = N - m$, starting at (0,0) and ending at (n_1, n_2) after q jumps. Introducing $h_k(x) = k(x+1)$ simplifies the collective action,

$$\hat{S}_1 |u_1, u_2\rangle = \sqrt{h_k(u_1)} |u_1 + 1, u_2\rangle,$$
$$\hat{S}_2 |u_1, u_2\rangle = \sqrt{h_k(u_2)} |u_1, u_2 + 1\rangle, \tag{10}$$

with $k = N - u_1 - u_2$. We follow the evolution on each decay path from $|0,0\rangle$ to $|n_1, n_2\rangle$. A path j is specified by a string $\alpha = (\alpha_N, \ldots, \alpha_{m+1})$ of length $q = N - m$, where $\alpha_k = 1$ (0) denotes a jump through $\hat{S}_1$ ($\hat{S}_2$). The number of distinct paths is $n_{\rm paths} = (n_1 + n_2)!/(n_1! n_2!)$.

Along any path j, the collapse operators generate a product containing n_1 factors from channel 1 and n_2 from channel 2. This gives a product $N \cdots (m+1) = N!/m!$ multiplied with a product $n_1! n_2!$, which we collect as $\mathcal{C}_{n_1,n_2} = (N! n_1! n_2! \Gamma_1^{n_1} \Gamma_2^{n_2}/m!)$. The non-Hermitian evolution picks up the total rates out of the states reached along path j,

$$\Lambda_k^{(j)} = \Gamma_1 h_k(u_1^{(j)}) + \Gamma_2 h_k(u_2^{(j)})$$
$$= k\left[\Gamma_1 (u_1^{(j)} + 1) + \Gamma_2 (u_2^{(j)} + 1)\right], \tag{11}$$

as illustrated in Fig. 2(b). Summing over all paths gives

$$p_{n_1,n_2}(t) = \mathcal{C}_{n_1,n_2} \left(e^{-\Lambda_N t} * \left[\sum_{j=1}^{n_{\rm paths}} e^{-\Lambda_{N-1}^{(j)} t} * \cdots * e^{-\Lambda_{m+1}^{(j)} t} \right] * e^{-\Lambda_m t} \right). \tag{12}$$

The endpoints $|0,0\rangle$ and $|n_1, n_2\rangle$ are common to all trajectories, so $\Lambda_N = N(\Gamma_1 + \Gamma_2)$ and $\Lambda_m = m[\Gamma_1(n_1+1) + \Gamma_2(n_2+1)]$ are path-independent. The Laplace transform $\tilde{p}_{n_1,n_2}(s)$ is obtained from Eq. (12) analogously to Eq. (7), now with a sum over paths,

$$\tilde{p}_{n_1,n_2}(s) = \mathcal{C}_{n_1,n_2} \sum_{j=1}^{n_{\rm paths}} \prod_{k=m}^{N} \frac{1}{s + \Lambda_k^{(j)}}, \tag{13}$$

with $m = N - n_1 - n_2$. For the stationary ground-manifold state $m = 0$, the final segment has $\Lambda_0^{(j)} = 0$ for every path. Hence the Laplace transform contains one factor $1/s$, which leads to the steady state

$$p^{(ss)}_{n_1,n_2} = \lim_{s \to 0} s \tilde{p}_{n_1,n_2}(s) = \mathcal{C}_{n_1,n_2} \sum_{j=1}^{n_{\rm paths}} \prod_{k=1}^{N} \frac{1}{\Lambda_k^{(j)}}. \tag{14}$$

Hence, the nontrivial stationary ground-manifold distribution follows directly from the same Laplace-space trajectory solution as the transient dynamics, without requiring an inverse Laplace transform or numerical long-time propagation.

As a simple example, let us consider $\Gamma_1 = \Gamma_2 = \Gamma/2$. The rates $\Lambda_k^{(j)} = \Gamma k(N - k + 2)/2$ become completely independent of the path, and one obtains $\prod_{k=1}^{N} \Lambda_k^{(j)} = (\Gamma/2)^N N!(N+1)!$, leading to the flat ground-state distribution for balanced decay,

$$p^{(ss)}_{n_1,n_2} = \frac{1}{N+1}. \tag{15}$$

The generalization to $d > 2$ collective decay channels, and analytic expressions for the stationary state $p^{(ss)}_{n_1,\ldots,n_d}$, are given in Supplemental Material [22].

Superradiant transient and stationary state—In Fig. 3(a) we show Dicke superradiance for d collective decay channels with balanced rates, $\Gamma_1 = \cdots = \Gamma_d = \Gamma/d$. For

balanced decay, all trajectories that reach a fixed excitation number m experience the same total non-Hermitian decay rate, independent of how the previous jumps were distributed among the d ground-state channels. The multichannel dynamics therefore collapse to an effective one-dimensional cascade in m. The emitted intensity $\mathcal{I}_{\mathrm{tot}}(t) = (\Gamma/d)\sum_\alpha \langle \hat{S}_\alpha^\dagger \hat{S}_\alpha \rangle$ (in units of $\hbar\omega$) is plotted versus time for increasing d. As d grows, the burst weakens and shifts to later times. In Fig. 3(b), we plot the total emitted peak intensity and delay time [36] as functions of d. We find

$$\frac{\mathcal{I}_{\mathrm{tot}}^{\max}}{\Gamma} \approx \frac{(N+d-1)^2}{4d+1}, \qquad \Gamma t_{\mathrm{peak}} \approx \frac{d\ln\left(\frac{N}{d}\right)}{N+d}. \quad (16)$$

The peak-intensity expression in Eq. (16) is obtained by fitting the peak values extracted from the exact analytical solution, whereas the peak time is calculated in Supplemental Material [22] from the expected time to reach the state with $m = (N+d)/2$. Equation (16) reproduces the standard $d = 1$ scaling and captures the $1/d$ suppression of the peak intensity for d equal decay channels. The delayed and weakened superradiant burst follows directly from the loss rate $[\Gamma/d]m(N-m+d)$ of a state with m excitations, which yields a parabolic scaling $\sim N^2/d$ around $m = (N+d)/2$ and therefore suppresses the peak as d increases.

For single-channel Dicke superradiance the stationary state is trivial, $|\psi(t\to\infty)\rangle = |g\rangle^{\otimes N}$. For $d = 2$, the stationary state is a distribution over ground states $|n_1, n_2\rangle$ with $n_1 + n_2 = N$ [Fig. 1(b) and Eq. (9)]. We provide a closed-form expression for $p^{(ss)}_{n_1,n_2}$ valid for any N and $\Gamma_{1,2}$ in Supplemental Material [22]. Writing these probabilities as $p^{(ss)}_{N-x,x}$ with $x = 0,\ldots,N$, we define the stationary state population fraction in $|g_2\rangle$ as $\bar{n}_2 = (1/N)\sum_{x=0}^{N} x p^{(ss)}_{N-x,x}$, with control parameter $r = \Gamma_2/\Gamma_1$; see Fig. 3(c).

First-order-like dissipative transition—The stationary state distribution $p^{(ss)}_{N-x,x}$ reached from the fully excited state resembles a first-order phase transition [37,38]. What we call a phase transition here is a nonanalyticity of the order parameter $\bar{n}_2(N,r)$ at $r = 1$ as $N\to\infty$, not necessarily accompanied by a spontaneous symmetry breaking as in equilibrium systems. The order parameter is $\bar{n}_2(N,r)$ and the control parameter is the decay-rate ratio r. At $r = 1$ symmetry fixes $\bar{n}_2 = 1/2$ for any N, while for $r \neq 1$ the distribution is strongly biased. In the limit $N\to\infty$, $\bar{n}_2(N,r)$ sharpens into a Heaviside step function, as in a first-order transition. The mechanism is simple: decay into a particular ground state $|g_\alpha\rangle$ enhances the probability that subsequent decays populate the same state, so an infinitesimal rate imbalance becomes amplified in the ground-state distribution. Quantitatively, the susceptibility at the balanced point follows in closed form as (see Supplemental Material [22])

$$\partial_r \bar{n}_2(N,r)|_{r=1} = \frac{\ln N}{6} + O(1). \quad (17)$$

However, the thermodynamic analogy breaks down here: because the number of accessible states grows linearly with N, the normalized distribution $p^{(ss)}_{N-x,x}$ appears locally flat as $N\to\infty$, corresponding to an effective $T = \infty$. The stationary behavior map onto a two-color Pólya urn with unequal reinforcement rates [39], which provides a natural stochastic-process description of the reinforcement mechanism underlying the logarithmically increasing susceptibility.

We note that generic symmetry-breaking perturbations may round the large-N nonanalytic behavior, so the present solution provides the permutation-symmetric limiting case for assessing the robustness of this transition.

Discussion and conclusions—We introduced a symbolic quantum-trajectory solution of Dicke superradiance with d competing collective decay channels. The method yields closed time-domain expressions for symmetric-state populations and observables as finite closed combinations of exponential terms with rates set by N and $\{\Gamma_\alpha\}$. For balanced multichannel emission we derived compact analytic scalings for the superradiant delay time and peak emission rate, Eq. (16), extending Dicke's $d = 1$ results to multilevel emitters. For two channels we found a sharp ground-manifold selection controlled by $r = \Gamma_2/\Gamma_1$, with logarithmically diverging susceptibility at the balanced point, Eq. (17), and a Heaviside-like order parameter in the limit $N\to\infty$.

Experimentally, crossed or polarization-resolved cavities enable tunable multichannel superradiance with adjustable r [28], while bad-cavity superradiance with cold atoms has been realized on narrow optical transitions [23,24]. In nanophotonic waveguide QED, guided modes provide permutation-symmetric reservoirs and polarization or multimode engineering provides tunable channel rates [29–31]. These settings allow initialization near $|e\rangle^{\otimes N}$ (or rapid pumping), control of r, and time-resolved detection of both the multichannel burst and the final ground-manifold distribution. The resulting winner-takes-all [11] ground-state selection resembles a dissipative many-body phase transition: the stationary state of the Liouvillian acquires a nonanalytic dependence on the ratio of cooperative decay rates, with a susceptibility that diverges logarithmically with N. This connects multichannel Dicke superradiance to experimentally studied nonequilibrium critical phenomena in driven-dissipative platforms [37,40–42], while keeping the control knob minimal (a ratio of collective decay rates).

Permutation-invariant local decoherence or pumping can instead be incorporated within weak-permutation-symmetry formulations [13–15,17]. In the trajectory picture, incoherent pumping introduces loops into the otherwise acyclic jump graph and therefore requires a resummation or recursive treatment, while coherent driving generally

replaces the scalar no-jump evolution terms by matrix-valued terms within the symmetric manifold, as encountered in fully collective driven models [43]. Generic emitter-dependent disorder or inhomogeneous couplings, by contrast, break the symmetry underlying the present exact solution. The model solved here therefore provides both an analytically tractable limit and a reference point for studying how such perturbations modify multichannel collective decay.

Acknowledgments—We acknowledge financial support from the Max Planck Society and the Deutsche Forschungsgemeinschaft (DFG, German Research Foundation)—Project-ID 429529648—TRR 306 QuCoLiMa ("Quantum Cooperativity of Light and Matter"). S. F. Y. acknowledges the NSF via PHY-2207972. This research was funded in whole or in part by the Austrian Science Fund (FWF) [Grant DOI: 10.55776/COE1].

Data availability—There are no publicly available research data or software supporting this manuscript. Requests for further information or data should be sent to the authors.

[1] R. H. Dicke, Coherence in spontaneous radiation processes, Phys. Rev. **93**, 99 (1954).
[2] V. V. Temnov and U. Woggon, Superradiance and subradiance in an inhomogeneously broadened ensemble of two-level systems coupled to a low-Q cavity, Phys. Rev. Lett. **95**, 243602 (2005).
[3] M. O. Scully and A. A. Svidzinsky, The super of superradiance, Science **325**, 1510 (2009).
[4] C. T. Lee, Exact solution of the superradiance master equation. Complete initial excitation, Phys. Rev. A **15**, 2019 (1977).
[5] C. T. Lee, Exact solution of the superradiance master equation. II. Arbitrary initial excitation, Phys. Rev. A **16**, 301 (1977).
[6] R. Holzinger and C. Genes, A compact analytical solution of the Dicke superradiance master equation via residue calculus, Z. Naturfor. A **80**, 673 (2025).
[7] R. Holzinger, N. S. Bassler, J. Lyne, F. G. Jimenez, J. T. Gohsrich, and C. Genes, Solving Dicke superradiance analytically: A compendium of methods, Phys. Rev. A **113**, 043718 (2026).
[8] R. T. Sutherland and F. Robicheaux, Superradiance in inverted multilevel atomic clouds, Phys. Rev. A **95**, 033839 (2017).
[9] A. Piñeiro Orioli, J. K. Thompson, and A. M. Rey, Emergent dark states from superradiant dynamics in multilevel atoms in a cavity, Phys. Rev. X **12**, 011054 (2022).
[10] S. J. Masson, J. P. Covey, S. Will, and A. Asenjo-Garcia, Dicke superradiance in ordered arrays of multilevel atoms, PRX Quantum **5**, 010344 (2024).
[11] W.-K. Mok, S. J. Masson, D. M. Stamper-Kurn, T. Zelevinsky, and A. Asenjo-Garcia, Ground-state selection via many-body superradiant decay, Phys. Rev. Res. **7**, L022015 (2025).
[12] A. Sivan and M. Orenstein, Adding photonic entanglement to superradiance by using multilevel atoms, Phys. Rev. Res. **7**, 033170 (2025).
[13] B. A. Chase and J. M. Geremia, Collective processes of an ensemble of spin-1/2 particles, Phys. Rev. A **78**, 052101 (2008).
[14] B. Q. Baragiola, B. A. Chase, and J. M. Geremia, Collective uncertainty in partially polarized and partially decohered spin-1/2 systems, Phys. Rev. A **81**, 032104 (2010).
[15] M. Xu, D. A. Tieri, and M. J. Holland, Simulating open quantum systems by applying SU(4) to quantum master equations, Phys. Rev. A **87**, 062101 (2013).
[16] Y. Zhang, Y.-X. Zhang, and K. Mølmer, Monte-Carlo simulations of superradiant lasing, New J. Phys. **20**, 112001 (2018).
[17] E. W. Lloyd, A. A. Ziolkowska, and J. Keeling, Permutation-symmetric quantum trajectories, arXiv:2605.11103.
[18] K. Mølmer, Y. Castin, and J. Dalibard, Monte Carlo wave-function method in quantum optics, J. Opt. Soc. Am. B **10**, 524 (1993).
[19] H. J. Carmichael, *An Open Systems Approach to Quantum Optics*, Lecture Notes in Physics Vol. 18 (Springer, Berlin, 1993).
[20] M. B. Plenio and P. L. Knight, The quantum-jump approach to dissipative dynamics in quantum optics, Rev. Mod. Phys. **70**, 101 (1998).
[21] A. J. Park, J. Trautmann, N. Šantić, V. Klüsener, A. Heinz, I. Bloch, and S. Blatt, Cavity-enhanced optical lattices for scaling neutral atom quantum technologies to higher qubit numbers, PRX Quantum **3**, 030314 (2022).
[22] See Supplemental Material at http://link.aps.org/supplemental/10.1103/5qcc-wfv6 for details on the adiabatic elimination in the bad-cavity limit, solving Dicke superradiance for more than two channels, balanced decay, steady-state ground-state distribution for two channels, analogy to dissipative quantum many-body phase transition as well as mean field and stochastic simulations for multichannel Dicke superradiance.
[23] J. G. Bohnet, Z. Chen, J. M. Weiner, D. Meiser, M. J. Holland, and J. K. Thompson, A steady-state superradiant laser with less than one intracavity photon, Nature (London) **484**, 78 (2012).
[24] M. A. Norcia and J. K. Thompson, Cold-strontium laser in the superradiant crossover regime, Phys. Rev. X **6**, 011025 (2016).
[25] M. A. Norcia, M. N. Winchester, J. R. K. Cline, and J. K. Thompson, Superradiance on the millihertz linewidth strontium clock transition, Sci. Adv. **2** (2016).
[26] M. A. Norcia, J. R. K. Cline, J. A. Muniz, J. M. Robinson, R. B. Hutson, A. Goban, G. E. Marti, J. Ye, and J. K. Thompson, Frequency measurements of superradiance from the strontium clock transition, Phys. Rev. X **8**, 021036 (2018).
[27] J. A. Mlynek, A. A. Abdumalikov, Jr., C. Eichler, and A. Wallraff, Observation of Dicke superradiance for two artificial atoms in a cavity with high decay rate, Nat. Commun. **5**, 5186 (2014).
[28] M. Brekenfeld, D. Niemietz, J. D. Christesen, and G. Rempe, A quantum network node with crossed optical fibre cavities, Nat. Phys. **16**, 647 (2020).

[29] A. Goban, C.-L. Hung, J. D. Hood, S.-P. Yu, J. A. Muniz, O. Painter, and H. J. Kimble, Superradiance for atoms trapped along a photonic crystal waveguide, Phys. Rev. Lett. **115**, 063601 (2015).

[30] P. Solano, P. Barberis-Blostein, F. K. Fatemi, L. A. Orozco, and S. L. Rolston, Super-radiance reveals infinite-range dipole interactions through a nanofiber, Nat. Commun. **8**, 1857 (2017).

[31] A. S. Sheremet, M. I. Petrov, I. V. Iorsh, A. V. Poshakinskiy, and A. N. Poddubny, Waveguide quantum electrodynamics: Collective radiance and photon-photon correlations, Rev. Mod. Phys. **95**, 015002 (2023).

[32] J. D. Brehm, A. N. Poddubny, A. Stehli, T. Wolz, H. Rotzinger, and A. V. Ustinov, Waveguide bandgap engineering with an array of superconducting qubits, npj Quantum Mater. **6**, 10 (2021).

[33] C. Liedl, F. Tebbenjohanns, C. Bach, S. Pucher, A. Rauschenbeutel, and P. Schneeweiss, Observation of superradiant bursts in a cascaded quantum system, Phys. Rev. X **14**, 011020 (2024).

[34] J. P. Clemens, L. Horvath, B. C. Sanders, and H. J. Carmichael, Collective spontaneous emission from a line of atoms, Phys. Rev. A **68**, 023809 (2003).

[35] H. Carmichael and K. Kim, A quantum trajectory unraveling of the superradiance master equation, Opt. Commun. **179**, 417 (2000).

[36] M. Gross and S. Haroche, Superradiance: An essay on the theory of collective spontaneous emission, Phys. Rep. **93**, 301 (1982).

[37] H. J. Carmichael, Breakdown of photon blockade: A dissipative quantum phase transition in zero dimensions, Phys. Rev. X **5**, 031028 (2015).

[38] G. Beaulieu, F. Minganti, S. Frasca, V. Savona, S. Felicetti, R. D. Candia, and P. Scarlino, Observation of first- and second-order dissipative phase transitions in a two-photon driven Kerr resonator, Nat. Commun. **16**, 1954 (2025).

[39] S. Janson, Functional limit theorems for multitype branching processes and generalized Pólya urns, Stoch. Proc. Appl. **110**, 177 (2004).

[40] T. Fink, A. Schade, S. Höfling, C. Schneider, and A. Imamoglu, Signatures of a dissipative phase transition in photon correlation measurements, Nat. Phys. **14**, 365 (2018).

[41] F. Minganti, A. Biella, N. Bartolo, and C. Ciuti, Spectral theory of Liouvillians for dissipative phase transitions, Phys. Rev. A **98**, 042118 (2018).

[42] L. M. Sieberer, M. Buchhold, and S. Diehl, Keldysh field theory for driven open quantum systems: A review, Rep. Prog. Phys. **79**, 096001 (2016).

[43] J. T. Reilly, S. B. Jäger, J. Cooper, and M. J. Holland, Fully collective superradiant lasing with vanishing sensitivity to cavity length vibrations, Phys. Rev. Lett. **136**, 143803 (2026).